ORIGINAL ARTICLE

Structural basis for the stability of a thermophilic methionine adenosyltransferase against guanidinium chloride

**Francisco Garrido · John C. Taylor ·
Carlos Alfonso · George D. Markham ·
María A. Pajares**

Abstract The methionine adenosyltransferase from the thermophile *Methanococcus jannaschii* is fully and irreversibly unfolded in the presence of guanidinium chloride. Unfolding of this dimeric protein is a three-state process in which a dimeric intermediate could be identified. The less stable secondary structural elements of the protein are the C-terminal ends of β-strands E2 and E6, as deduced from the behavior of tyrosine to tryptophan mutants at residues 72 and 170, which are located in the subunit interface. Unraveling of these elements at the monomer interface may soften intersubunit interactions, leading to the observed 85% activity loss. Accumulation of the intermediate was associated with maintenance of residual activity, an increase in the elution volume of the protein upon gel filtration and a decrease in the sedimentation coefficient. Elimination of the remaining enzymatic activity occurred in conjunction with a 50% reduction in helicity and fluorescence alterations illustrating a transient burial of tryptophans at β-strands E2, E3 and E9. The available 3D-model predicted that these β-strands are involved in the central and N-terminal domains of the monomer structure. Severe perturbation of this area of the monomer–monomer interface may destroy the remaining intermolecular interactions, thus leading to dissociation and aggregation. Finally, transition to the denatured state includes completion of the changes detected in the microenvironments around tryptophans included at α-helixes H5 and H6, the loops connecting H5–E8 and E9, β-strands E3 and E12.

Abbreviations

MAT	Methionine adenosyltransferase
Mj-MAT	Methionine adenosyltransferase from *Methanococcus jannashii*
BsMAT	Methionine adenosyltransferase from *Bacillus subtilis*
MATα2	Catalytic subunit of mammalian methionine adenosyltransferase II
MAT I	Mammalian homo-tetramer of catalytic MATα1 subunits
MAT III	Mammalian homo-dimer of catalytic MATα1 subunits
CD	Circular dichroism
IPTG	Isopropyl β-D-thiogalactoside
GCl	Guanidinium chloride
ANS	8-Anilinonaphthalene-1-sulphonic acid

F. Garrido · M. A. Pajares (✉)
Instituto de Investigaciones Biomédicas "Alberto Sols"
(CSIC-UAM), Arturo Duperier 4, 28029 Madrid, Spain
e-mail: mapajares@iib.uam.es

J. C. Taylor · G. D. Markham
Institute for Cancer Research, Fox Chase Cancer Center,
333 Cotman Avenue, Philadelphia, PA 19111, USA

C. Alfonso
Centro de Investigaciones Biológicas (CSIC),
Ramiro de Maeztu 9, 28040 Madrid, Spain

Introduction

S-adenosylmethionine (AdoMet) was discovered by Cantoni as the methyl donor for the biosynthesis of N^1-methylnicotinamide (Cantoni 1951). Subsequently AdoMet has been shown to donate its methyl group in the large variety of

transmethylation reactions that consume up to 95% of the cellular content of the molecule (Cantoni 1975). In addition, other parts of AdoMet can be transferred in the synthesis of various biological compounds. These include the amino-carboxypropyl group for the synthesis of hypermodified tRNA nucleosides (Nishimura et al. 1974); the aminopropyl group (after AdoMet decarboxylation) for the synthesis of polyamines, plant hormones or signaling molecules of Gram negative bacteria (Sufrin et al. 2009); the 5′-deoxyadenosyl radical used by SAM radical proteins to generate vitamins, antioxidants and photosynthetic pigments (Frey et al. 2008); and the amino, ribosyl and carboxylic groups in other less common reactions (Eisenberg and Stoner 1971; Dolnick et al. 2003; Van Lanen and Iwata-Reuyl 2003). Despite the importance of AdoMet to all cells, there is only one known reaction for its synthesis, which is catalyzed by methionine adenosyltransferases (MATs).

MATs use methionine and ATP to produce AdoMet in a reaction that needs Mg^{2+} and K^+ ions and which is accompanied by a tripolyphosphatase activity (Markham and Pajares 2009). Phylogenetically, these oligomeric proteins appear in all types of organisms, except some parasites that seem to obtain AdoMet from their host by using appropriate transporters (Sanchez-Perez et al. 2004). The catalytic subunits present a very high degree of sequence conservation ($\sim$80%; 59% residue identity) among Bacteria and Eukarya. Their active sites are located at the interface between monomers in the dimer with residues of both subunits contributing to catalysis (Markham and Pajares 2009). MATs appear either as hetero- (mammalian MAT II) or homo-oligomers, and their preferred association state seems to be as tetramers, except for mammalian MAT III and the archaeal MATs that are dimers (Sanchez-Perez et al. 2004; Markham and Pajares 2009). Archaeal MATs show very low sequence conservation ($\sim$20% at the amino acid level) as compared to bacterial and eukaryotic proteins, but conservation is concentrated on residues involved in catalysis (Graham et al. 2000; Lu and Markham 2002). In addition, their maximal catalytic activity is obtained at $\geq$55°C, the T_m for mammalian MAT I/III inactivation (Iloro et al. 2004).

Structural information about the MAT family members is restricted to crystal structures for the *E. coli* (Takusagawa et al. 1996; Markham and Pajares 2009) and mammalian MATs (Gonzalez et al. 2000, 2003) (pdb unpublished 2P02 and 2OBV). All of the catalytic subunits are α/β type proteins, which are organized in three domains composed of non-consecutive sections of the sequence, and the monomers interact through a large flat hydrophobic surface to form the active dimers (Markham and Pajares 2009). These characteristics suggest that independent folding of each domain cannot be expected during protein synthesis. Moreover, complete folding of the monomer into its native structure should be precluded in the aqueous cytoplasm and can only be achieved through concomitant subunit association. Assisted folding might be a way to overcome these problems and, in fact, MAT was identified as one of the obligate substrates for chaperonin GroEL/GroES catalyzed folding in *E. coli* (Fujiwara et al. 2010; Houry et al. 1999). Collected studies on oligomeric proteins show that they prefer multi-state folding processes involving mono- and/or multimeric intermediates (Neet and Timm 1994; Batey et al. 2006), and MATs are not an exception to this rule (Gasset et al. 2002; Kamarthapu et al. 2008; Garrido et al. 2009). In fact, in vitro studies of the folding of mesophilic MATs have detected mono- and dimeric intermediates, as well as kinetic intermediates whose structural characteristics are not completely established (Gasset et al. 2002; Sanchez del Pino et al. 2002; Sanchez-Perez et al. 2003; Kamarthapu et al. 2008). Previous data on urea-unfolding of *M. jannaschii* MAT (Mj-MAT) allowed identification of mono- and dimeric intermediates, although only partial unfolding of the protein was achieved (Garrido et al. 2009). Therefore, the present study was undertaken to further analyze the changes needed for Mj-MAT unfolding and the structural basis for the increased Mj-MAT stability as compared to its mesophilic counterparts.

Materials and methods

Protein expression and purification

Escherichia coli BL21(DE3) competent cells were transformed with either the pMJ1208-1 plasmid or the mutant plasmids (Garrido et al. 2009). A single colony was used to inoculate 5 l of culture media (LB plus 50 µg/ml ampicillin) that was grown at 37°C until $A_{595} \sim 0.6$. Expression was induced for 3 h at 37°C using 0.5 mM isopropyl β-D-thiogalactoside (IPTG; Ambion, Austin, TX, USA). Cells were harvested by centrifugation and stored at –80°C until use. Cell lysis was performed by sonication (30 cycles, 30 s on/off) in an ice bath, and Mj-MAT purification was carried out as previously described by Lu and Markham (2002). Protein concentration was determined using the A_{280} of the sample after 30 min incubation in 6 M GCl (Calbiochem, La Jolla, CA, USA) and using the calculated extinction coefficients previously reported (Garrido et al. 2009).

Site-directed mutagenesis

Mutagenesis of Mj-MAT was carried out using the QuikChange site-directed mutagenesis method (Stratagene, La Jolla, CA, USA), following manufacturer's instructions.

The W387F mutant was constructed in the vector pMJ1208-1 and the rest of the mutants were prepared on this W387F background plasmid and characterized as described previously (Garrido et al. 2009). Mutations were verified by automatic sequencing.

GCl incubation conditions

Purified Mj-MAT (5–250 μg/ml) was incubated for 1–24 h in 50 mM Tris/HCl pH 8, 50 mM KCl, 10 mM MgSO$_4$ (buffer A) containing different concentrations of GCl (0–6 M). Refolding was induced by either sample dilution or dialysis to the desired GCl concentration using buffer A. Once the irreversibility of the unfolding process was established, the incubations were performed routinely o/n at 23°C.

MAT activity assay

Mj-MAT activity in denaturation assays was measured at 55°C as described previously (Garrido et al. 2009), using a protein concentration of 0.05 mg/ml and the standard MAT reaction mixture in a final volume of 250 μl. Controls were carried out including variable concentrations of KCl (0–4 M). Characteristic concentrations at the midpoint of denaturation transitions ($D_{50\%}$) were calculated using GraphPad Prism v. 5.0 (GraphPad Software, San Diego, CA, USA). The equations used for fitting of the data were

1. Two-state unfolding:

$$Y = U + \frac{(N - U)}{(1 + 10^{(D^1 - X)})}$$

2. Three-state unfolding:

$$Y = U + (N - U)\left[\frac{(N - I)}{(1 + 10^{(X - D^1)})} + \frac{1 - (N - I)}{(1 + 10^{(X - D^2)})}\right]$$

where N, U and I are the values of the parameter measured for the native (0 M GCl), inactive or unfolded (6 M GCl) and intermediate states (at plateau), respectively; D^1 and D^2 are the denaturant concentrations at midpoint of the transitions; X is the denaturant concentration; and Y the value of the parameter measured (activity, fluorescence, etc.) at the different denaturant concentrations tested.

Intrinsic fluorescence experiments

Mj-MAT samples (5–100 μg/ml) in different concentrations of GCl (0–6 M) in buffer A were incubated overnight at 23°C. Fluorescence spectra were recorded between 300 and 400 nm in a photon counting SLM-8000 spectrofluorometer at 25°C, using 0.5 × 0.5 cm cuvettes after excitation at 295 nm, with excitation and emission slit widths

of 2.5 and 5 nm, respectively. The only exception was the W387F mutant, which only contains tyrosines, and hence was excited at 275 nm. The fluorescence signal for the protein was corrected by subtraction of the solvent signal. The ratio I_{330}/I_{355} was calculated to obtain a measurement of the average exposure of the tryptophan residues to the solvent. Calculation of $D_{50\%}$ values was performed as described above for data from enzyme activity measurements.

ANS binding

A stock solution 100 mM 8-anilinonaphthalene-1-sulphonic acid (ANS; Sigma Chemical Co, St. Louis, MO, USA) was prepared in methanol, and its concentration adjusted using the A$_{370}$ and a molar extinction coefficient of 6,800 M^{-1} cm^{-1}. ANS was added to pre-equilibrated Mj-MAT unfolding reactions (1 ml, 50 μg/ml) or to control reactions without protein, to achieve a final concentration of 0–40 μM; the final methanol concentration in the sample was 0.4% (v/v). Changes in ANS emission at 470 nm due to protein binding were monitored upon excitation at 380 nm after 1-h incubation in the dark. The increase in fluorescence emission was determined from the spectra recorded between 400 and 600 nm, after baseline and instrumental factor corrections.

Circular dichroism experiments

GCl denatured and refolded Mj-MAT samples were prepared as described for activity and fluorescence measurements, but at 0.1–0.25 mg/ml protein concentrations for far-UV CD. Analysis of the near-UV CD signals was precluded due to the absence of a defined signature for the mutants, ellipticity signals at 295 nm being negligible (Garrido et al. 2009). Far-UV spectra were recorded on a Jasco J-720 spectropolarimeter at 25°C, using 0.1 cm pathlength cuvettes. After baseline subtraction the observed ellipticities were converted to mean residue ellipticities (θ_{mrw}) on the basis of a mean molecular mass per residue of 110 Da. A minimum of five spectra was taken for each sample. $D_{50\%}$ values were calculated using GraphPad Prism v. 5.0, as for activity and fluorescence curves.

Gel filtration chromatography

Unfolded Mj-MAT samples (0–4 M GCl; 500 μl) were prepared at 0.5 mg/ml and loaded on a Biogel A 1.5 m column (45 ml; Bio-Rad Laboratories, Hercules, CA, USA) equilibrated in buffer A containing the appropriate GCl concentrations. Elution was carried out at 23°C using the corresponding equilibration buffers at 7.5 ml/h and 0.5 ml fractions were collected for protein detection using

the BCA kit (Pierce, Rockford, IL, USA). The standards (Sigma Chemical Co, St. Louis, MO, USA and GE Healthcare Europe GmbH, Barcelona, Spain) used and their elution volumes were blue dextran (2,000 kDa; 18 ml), tyroglobulin (669 kDa; 21 ml), apoferritin (443 kDa; 23 ml), β-amylase (200 kDa; 25 ml), alcohol dehydrogenase (150 kDa; 26.5 ml), BSA (66.2 kDa; 28 ml), conalbumin (75 kDa; 30 ml), carbonic anhydrase (29 kDa; 31 ml) and ATP (507 Da; 39.5 ml).

Sedimentation velocity experiments

Mj-MAT samples (0.5 mg/ml) were incubated in the presence of 0–3 M GCl. Sedimentation velocity runs were carried out at 48,000 rpm and 20°C in an XL-1 analytical ultracentrifuge (Beckman Coulter, Inc., Fullerton, CA, USA) with an UV–Vis detection system, using an An50Ti rotor and 12 mm double-sector centerpieces. Absorbance scans (0.003 cm step size) were taken at 280 nm. Differential sedimentation-coefficient distributions, c(s), were calculated by least squares boundary modeling of sedimentation velocity data using the program SEDFIT (Schuck 2000; Schuck et al. 2002). The values obtained from this analysis were corrected for solvent composition and temperature to obtain $s_{20,w}$ using the public domain software SEDNTERP, retrieved from the RASMB server (Laue et al. 1992).

Mj-MAT structural model

The secondary structure predictions for Mj-MAT and the previously described structural model (Garrido et al. 2009)

were used in this work for discussion of the data. This model lacks 18 residues of the C-terminal end, finishing at residue 388.

Results

Previous studies of Mj-MAT stability showed the resistance of this protein to urea unfolding. In fact, after 24 h incubation in 8 M denaturant Mj-MAT monomers were obtained that still retained a large proportion of their native secondary and tertiary structures (Garrido et al. 2009). Therefore, the purpose of the present study was to further analyze the changes required to obtain Mj-MAT complete unfolding and to reveal the structural features that provide this stability. Thus, a stronger denaturant agent was needed and we selected GCl, which combines ionic effects with those of urea (Mayr and Schmid 1993; Akhtar et al. 2002). Incubations in the presence of GCl (0–6 M) were carried out for different time periods (1–24 h) and the reversibility of the process was tested both by dilution and dialysis of the samples. However, neither procedure allowed recovery of Mj-MAT activity or the original fluorescence signal. Thus, the unfolding process induced by GCl was irreversible.

The effect of GCl on Mj-MAT was followed using activity measurements (Fig. 1a). Reduction of activity was observed upon addition of the lowest denaturant concentration tested (0.05 M GCl) and the enzyme was completely inactivated already at 2 M GCl. The inactivation profiles showed two transitions, the first (0.05–1 M) corresponding to a decrease of ~85% in the AdoMet

Fig. 1 Effects of guanidinium chloride on Mj-MAT followed by activity measurements. The effect of different guanidinium chloride concentrations on Mj-MAT activity was followed at 50 μg/ml protein (a). These effects were also analyzed in the mutant proteins that included a single tryptophan and the W387F background mutant in which they were introduced (b–d). The figure shows results of a typical experiment carried out in triplicate (mean ± SD)
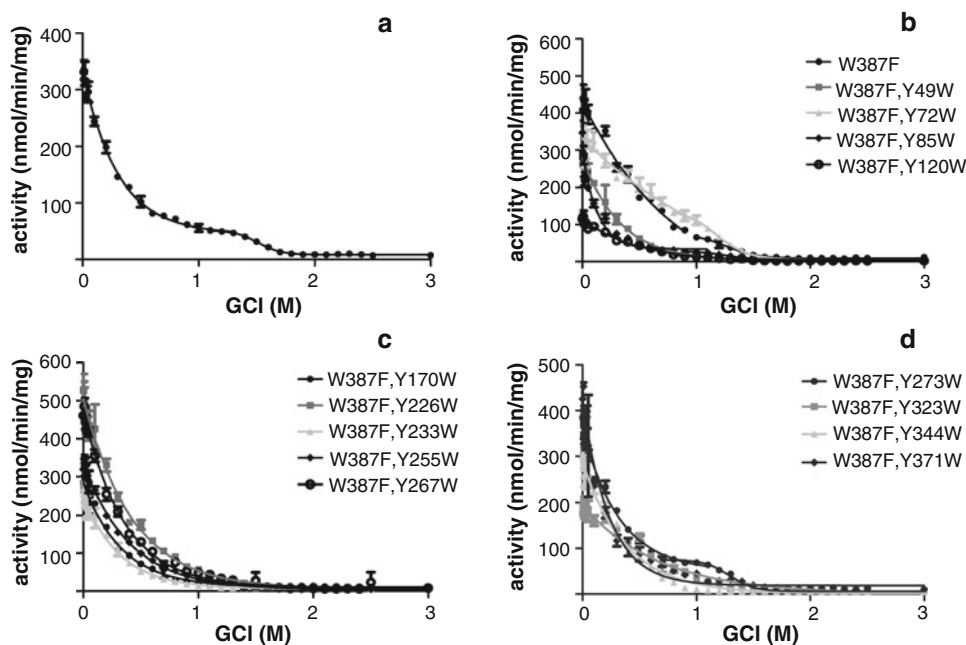
Table 1 Wild type Mj-MAT unfolding by GCl was followed at several protein concentrations using different techniques and the denaturant concentrations at midpoint of transitions calculated

|		Mj-MAT (μg/ml)	GCl unfolding[a]	
			$D_{50\%}^1$ (M)	$D_{50\%}^2$ (M)
Activity		50	0.21 ± 0.01	1.51 ± 0.01
Fluorescence	$I_{330/355}$	5^b	–	1.89 ± 0.05
		50	1.67 ± 0.01	2.63 ± 0.09
		100	1.74 ± 0.09	3.09 ± 0.05
	λ_{max}	50	0.76 ± 0.18	2.71 ± 0.05
CD		200	1.63 ± 0.02	3.45 ± 0.07
		250	1.72 ± 0.03	3.45 ± 0.07

Results are shown as the mean ± SD of three independent experiments

[a] Values for the denaturant concentrations at midpoint of the transitions were calculated using equations for a three- state mechanism

[b] Values for the denaturant concentrations at midpoint of the transitions were calculated using equations for a two-state mechanism

synthesizing capacity of the protein. Data at the plateau (1–1.4 M GCl) between both transitions indicated a residual 15% activity that disappeared during the second transition (1.4–2 M). Denaturant concentrations at midpoints of transitions were calculated and appear listed in Table 1. Controls performed in the presence of equivalent KCl concentrations showed no effect on activity in this concentration range (0–4 M).

Two transitions were also observed when the Mj-MAT GCl-unfolding process was followed by fluorescence (Fig. 2) and far-UV CD spectroscopies (Fig. 3). The plateau defining the native state was found between 0 and 1.2 M denaturant, and the denatured state was detected above 4 M GCl. The fluorescence spectrum of the wild type protein in the presence of 4–6 M denaturant showed a 70% decrease in intensity (Fig. 2a inset), and its λ_{max} was already red-shifted to 355 nm at 4 M GCl (Fig. 2b), demonstrating a total exposure of the native W387 residue to the solvent. CD spectra of the protein showed disappearance of the typical signature for the presence of secondary structure above 4 M GCl, the ellipticity signal at 220 nm being reduced by 85% (Fig. 3). A third plateau, suggestive of the existence of an intermediate, was detected between 2 and 2.5 M GCl using the I_{330}/I_{355} fluorescence ratio (Fig. 2a) and the far-UV CD signal at 220 nm (Fig. 3), whereas this plateau occurred between 1 and 2 M when followed by the changes in λ_{max} (Fig. 2b). Thus, these data suggested a three-state unfolding process with the characteristic denaturant concentrations at midpoint of transitions listed in Table 1.
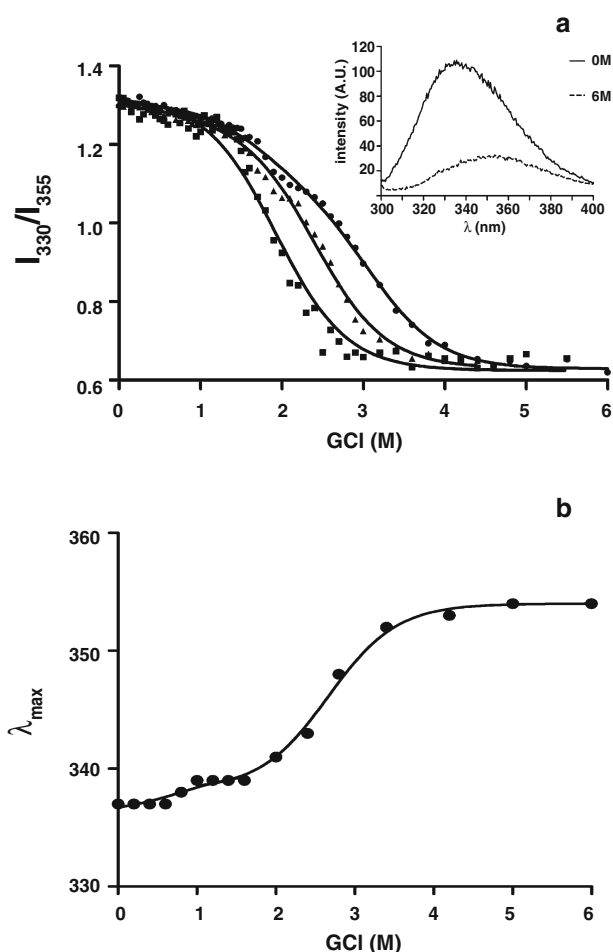
Fig. 2 Unfolding of Mj-MAT followed by fluorescence. The effect of guanidinium chloride on Mj-MAT denaturation was studied by fluorescence spectroscopy ($\lambda_{ex} = 295$ nm) at different protein concentrations: *filled square* 5 μg/ml; *filled triangle* 50 μg/ml and *filled circle* 100 μg/ml (**a**). The *inset* shows fluorescence spectra of Mj-MAT at 0 (*continuous line*) and at 6 M denaturant (*dotted line*). Displacement of the protein λ_{max} at 50 μg/ml as the guanidinium chloride concentration increases is depicted in (**b**). The results were fit to the presence of several transitions using GraphPad Prism

Changes in the association state of the Mj-MAT dimer induced by GCl-unfolding were followed by gel filtration chromatography (Fig. 4a). An increase in the elution volume of the protein was observed on a calibrated gel filtration chromatography column at 1 M GCl, the calculated mass of this species corresponding to a globular protein of apparently 60.4 kDa. Such an elution volume, intermediate between those expected for the dimer (90 kDa) and for a globular monomer (~ 44 kDa), could be ascribed to the presence of both interconverting species (dimer and monomer) or to changes in dimer or monomer shape. The presence of high-Mr species was detected when the chromatography was performed at concentrations above 2 M denaturant. Examination of GCl effects by sedimentation velocity indicated a reduction in the $s_{20,w}$ value of the
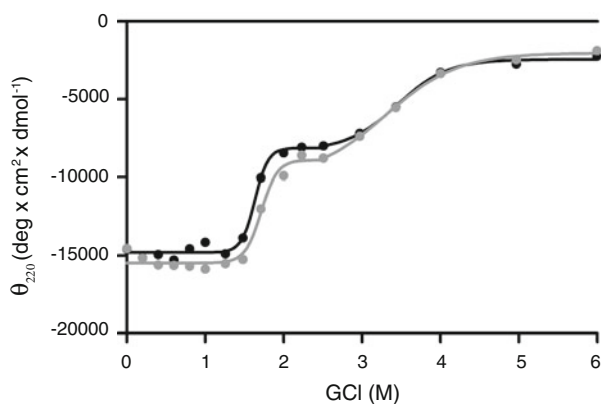
Fig. 3 Unfolding of Mj-MAT followed by far-UV circular dichroism. The effect of guanidinium chloride on wild type Mj-MAT denaturation was studied at 200 (*dark filled circle*) and 250 μg/ml (*grey filled circle*). The results were fit to the presence of either one or two transitions using GraphPad Prism. The figure shows the results of a typical experiment

protein from 5.8 ± 0.1 to 2.3 ± 0.1 at 0 and 3 M denaturant, respectively (Fig. 4b). This analysis also revealed the presence of both dimeric and monomeric species in a narrow GCl range (1–1.5 M) (Fig. 4c).

Comparison of the results obtained by the different techniques indicated that the main inactivation of Mj-MAT (0–1 M) occurred in coincidence with minor changes in λ_{max} and no changes in the fluorescence intensity ratio or ellipticity (Figs. 1, 2, 3). Data at the concentration range (1–1.5 M) of the inactivation plateau indicated the presence of species with $s_{20,w}$ values of 4.7 ± 0.1 and 3.5 ± 0.1 compatible with the elution behavior observed on gel filtration chromatography. The fact that residual activity is still observed (1–1.4 M) suggested the dimeric composition of one of these species, as this is the minimum association state required for catalysis. The next GCl concentration range (1.5–2.5 M) coincided with numerous alterations in the protein's properties, including the final inactivation of the protein, initial changes in λ_{max} (Fig. 2b), as well as in the average exposure of the W387 residue (Fig. 2a), alterations in helicity (Fig. 3), and accumulation of both the low $s_{20,w}$ species observed by ultracentrifugation (Fig. 4c) and the high-Mr forms that were observed upon gel filtration chromatography (Fig. 4a). ANS binding was only observed at millimolar concentrations, indicating that all the Mj-MAT species detected had a very low affinity for the dye. The 2.5–4 M GCl concentration interval included the largest decrease in the I_{330}/I_{355} ratio ($\sim 70\%$) (Fig. 2a), the major displacement in the λ_{max} (Fig. 2b) and the final reduction in the far-UV CD signal (Fig 3), but no further changes in the sedimentation coefficient (Fig. 4b, c) occurred. Most importantly, the fluorescence changes were dependent on the protein concentration as also occurred in the first CD
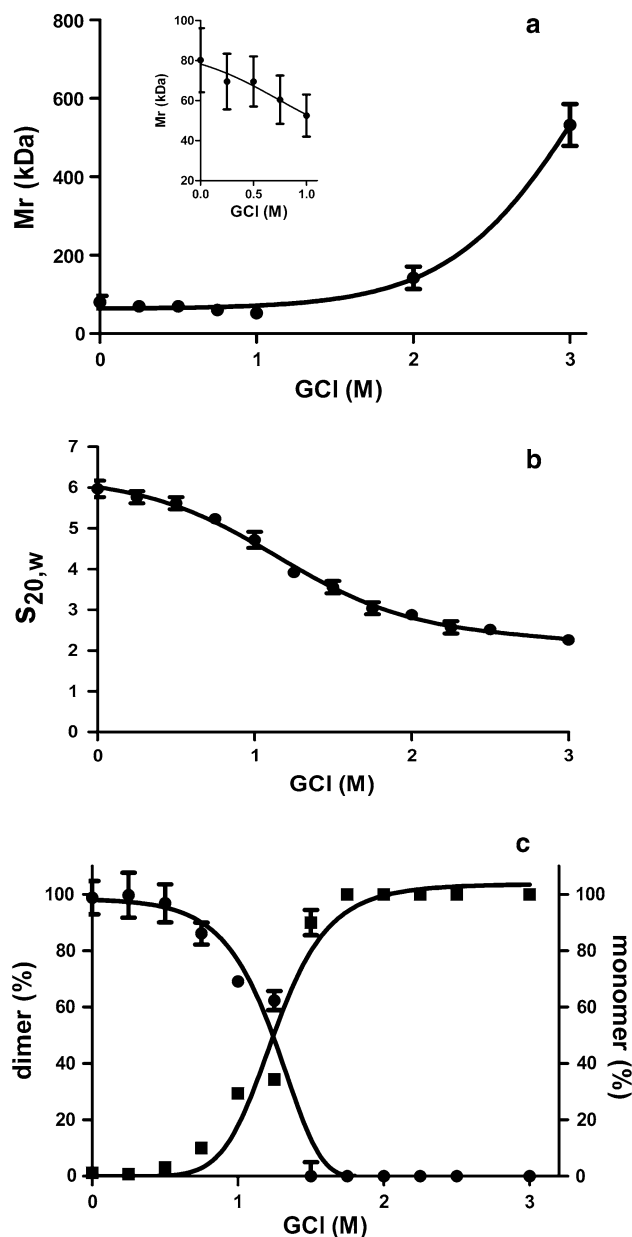
Fig. 4 Guanidinium chloride denaturation of Mj-MAT followed by gel filtration chromatography and sedimentation velocity. Samples (500 μl) of Mj-MAT (0.5 mg/ml) were incubated in the presence of guanidinium chloride, and used both for gel filtration chromatography or sedimentation velocity experiments. **a** The estimated Mr calculated from gel filtration profiles on a calibrated column; the inset highlights the Mr changes in the 0–1 M GCl range. **b** The calculated sedimentation coefficients of the main species detected in sedimentation velocity experiments. **c** The percentage of the species detected by sedimentation velocity. The figure presents results (mean ± SD) of a typical experiment

transition (Table 1). All these data together suggested initial accumulation of a compact dimeric intermediate retaining low activity, followed by dimer dissociation, all of these events taking place in a narrow range of denaturant concentrations. Detection of monomeric species by
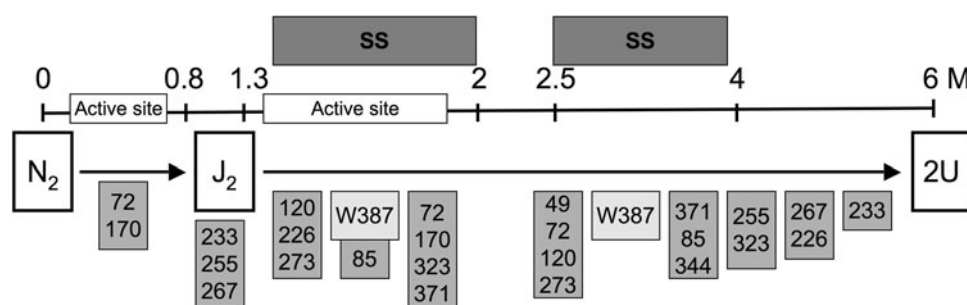
Fig. 5 Schematic representation of the changes observed on Mj-MAT secondary structure elements according to their behavior toward guanidinium chloride. The native dimer (N_2), the intermediate (J_2), and the unfolded state (U) are presented. The figure indicates the range of denaturant at which changes in activity (indicated as active site), in secondary structure (SS) or in the tertiary structure around tryptophans (shown by the residue number) take place. Moreover, concentration intervals at which important alterations are detected appear indicated. Events corresponding to wild type Mj-MAT are listed as W387

sedimentation velocity at the denaturant range where high-M_r forms eluted by gel permeation chromatography suggested that these monomers are prone to aggregation. Thus, the results suggested an irreversible three-state GCl-unfolding of Mj-MAT, including a dimeric intermediate (J_2) (Fig. 5).

In order to provide fluorescent probes throughout the protein sequence 13 tyrosine to tryptophan mutants were previously prepared on a Mj-MAT tryptophan-free variant (W387F) (Garrido et al. 2009). All these mutants were active and dimeric, and showed no dramatic alterations in their affinity for the substrates or far-UV CD spectra due to mutations. Analysis of the effect of GCl on the activity of the mutants revealed that most of them differed from the wild type behavior and showed a single inactivation transition (Fig. 1; Table 2). In fact, only W387F, W387F–Y72W, W387F–Y85W and W387F–Y273W exhibited two inactivation transitions. Comparison of the $D_{50\%}$ for the mutants and wild type revealed that the first transition shown by W387F–Y85W occurred at lower denaturant concentrations than that of the wild type, whereas those of W387F and W387F–Y72W occurred at higher values (Fig. 1; Table 2). Among the mutants showing a single transition, most exhibited $D_{50\%}$ values between $D_{50\%}^1$ and $D_{50\%}^2$ of the wild type enzyme. On the other hand, all the mutants showing a three-state behavior in activity measurements also exhibited second transitions with higher susceptibility to GCl denaturation than the wild type (Table 2).

The mutants included a single tryptophan in different secondary structure elements of the protein, thus allowing the selective observation of changes in those specific elements by fluorescence. Fluorescence spectra of the mutants in 6 M GCl showed complete exposure to the solvent of the corresponding tryptophans, as defined by λ_{max} values of 350–355 nm. The denaturation curves, followed by the average exposure of the tryptophans, suggested a three-state unfolding for most of the proteins. However, W387F–

Table 2 Guanidinium chloride effects on Mj-MAT activity defined by denaturant concentrations at midpoint of transitions

Protein	GCl unfolding[a]	
	$D_{50\%}^1$ (M)	$D_{50\%}^2$ (M)
Wild type[b]	0.21 ± 0.01[b]	1.51 ± 0.01[b]
W387F	0.59 ± 0.32	1.3 ± 0.02
W387F–Y49W	0.23 ± 0.02	–
W387F–Y72W	0.6 ± 0.34	1.19 ± 0.11
W387F–Y85W	0.11 ± 0.07	1.21 ± 0.01
W387F–Y120W	0.36 ± 0.13	–
W387F–Y170W	0.23 ± 0.02	–
W387F–Y226W	0.29 ± 0.02	–
W387F–Y233W	0.22 ± 0.01	–
W387F–Y255W	0.28 ± 0.01	–
W387F–Y267W	0.25 ± 0.01	–
W387F–Y273W	0.21 ± 0.02	1.29 ± 0.01
W387F–Y323W	0.51 ± 0.02	–
W387F–Y344W	0.3 ± 0.02	–
W387F–Y371W	0.41 ± 0.07	–

[a] Results were fit to the presence of two- or three states and are shown as the mean ± SD of a typical experiment carried out in triplicate at 50 µg/ml protein concentration

[b] Data from Table 1

Y49W and W387F–Y344W showed only one transition, whereas the data for W387F–Y72W fit to the presence of three transitions (Table 3; Fig. 6). Again, the susceptibility to the denaturant varied among mutant proteins, and hence a set with lower resistance to GCl than the wild type was found. This included (listed according to the lowest to the highest susceptibility): (1) W387F–Y72W, W387F–Y170W and W387F–Y255W; (2) W387F–Y233W; and (3) W387F–Y120W, W387F–Y226W, W387F–Y267W and W387F–Y273W. In addition, a delayed first transition was observed for: (1) W387F–Y323W and W387F–Y371W; (2) W387F–Y49W; and (3)

Table 3 Denaturant concentrations at midpoint of the transitions for Mj-MAT unfolding curves followed by the ratio of fluorescence intensities

Protein	GCl unfolding[a]		
	$D_{50\%}^{1}$ (M)	$D_{50\%}^{2}$ (M)	$D_{50\%}^{3}$ (M)
Wild type[b]	1.67 ± 0.01[b]	2.63 ± 0.09[b]	–
W387F	1.58 ± 0.21	3.03 ± 0.38	–
W387F–Y49W	2.47 ± 0.04	–	–
W387F–Y72W	0.63 ± 0.05	1.72 ± 0.08	2.56 ± 0.06
W387F–Y85W	1.67 ± 0.01	2.82 ± 0.06	–
W387F–Y120W	1.53 ± 0.01	2.55 ± 0.08	–
W387F–Y170W	0.5 ± 0.04	1.72 ± 0.02	–
W387F–Y226W	1.55 ± 0.02	3.41 ± 0.04	–
W387F–Y233W	1.06 ± 0.03	3.74 ± 0.01	–
W387F–Y255W	0.89 ± 0.26	3.04 ± 0.05	–
W387F–Y267W	1.37 ± 0.02	3.29 ± 0.08	–
W387F–Y273W	1.5 ± 0.01	2.59 ± 0.09	–
W387F–Y323W	1.79 ± 0.06	3.18 ± 0.18	–
W387F–Y344W	2.89 ± 0.06	–	–
W387F–Y371W	1.93 ± 0.03	2.67 ± 0.13	–

[a] The I_{330}/I_{355} fluorescence ratios for each protein were analyzed at 50 µg/ml upon excitation at 295 nm, except for W387F that was excited at 275 nm. The table shows the mean $\pm$ SD of $D_{50\%}$ values obtained from a typical experiment

[b] Data from Table 1

W387F–Y344W. Regarding the second transition, the behavior of the mutants can be also grouped in several categories as compared to the wild type (Table 3). Two mutants, W387F–Y72W and W387F–Y170W were more susceptible to the denaturant, their $D_{50\%}^{2}$ values corresponding to that of $D_{50\%}^{1}$ for the wild type. Moreover, these mutants both showed higher susceptibility to GCl during the first transition. Second transitions displaced to higher denaturant concentrations were also observed for a set of mutants (the lowest to the highest): (1) W387F–Y85W, W387F–Y255W, W387F–Y323W which show $D_{50\%}^{2}$ close to the $D_{50\%}^{1}$ exhibited by W387F–Y344W; (2) W387F–Y226W and W387F–Y267W; and (3) W387F–Y233W. The third transition noticed in W387F–Y72W exhibited a $D_{50\%}^{3}$ lower than that of $D_{50\%}^{2}$ for the wild type.

A close inspection of the GCl dependence of the fluorescence ratio for W387F–Y72W, W387F–Y85W and W387F–Y273W revealed a transient burial of the corresponding tryptophan between 1.5 and 2.5 M denaturant (Fig. 6c), a concentration range that included the first transition and the plateau observed for the wild type. Thus, the changes taking place in the microenvironments around the structural elements containing these three residues made them less exposed to the solvent in the intermediate state. The presence of a negligible near-UV CD signature
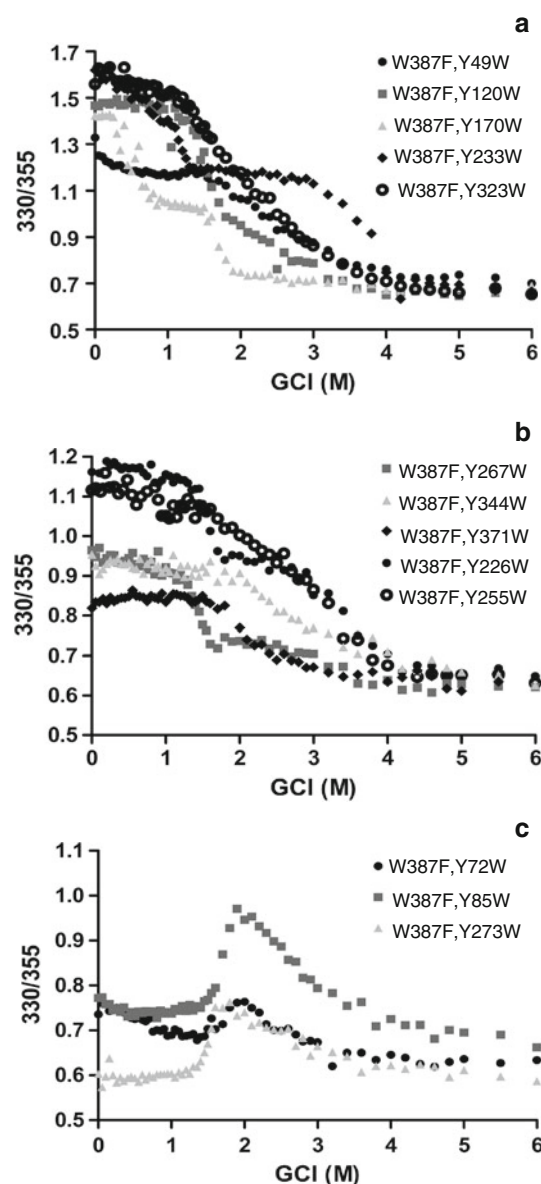
Fig. 6 Guanidinium chloride effects on the fluorescence of single tryptophan mutants. The denaturant (0–6 M) effects on the tertiary structure around tryptophans was analyzed by fluorescence upon excitation at 295 nm. The ratio of emission at 330/355 was followed in each case to analyze the degree of solvent exposure of the residue of interest upon denaturation

in the mutants precluded the use of this technique to corroborate these data. Inactivation by GCl preceded changes in the tertiary structure for all the mutants, independently of the secondary structure elements at which they were located, as occurred for the wild type protein. In fact, no mutant showed tertiary structure alterations at GCl concentrations <1 M, at which the main activity loss for the wild type was already produced (Figs. 1, 6). In contrast, the remaining activity disappeared after structural modifications around residues 72, 170, 233, 255 and 267 had taken place (Tables 2, 3).

Discussion

The archaeal Mj-MAT is a representative of a newly discovered class of MATs with very low sequence conservation when compared with the highly conserved bacterial and eukaryotic counterparts ($\sim 20\%$ identity at the amino acid level vs. 59% identity between E. coli and human enzymes) (Sanchez-Perez et al. 2004). In fact, only the active site residues are conserved thus allowing preservation of the reaction mechanism. However, maintenance of the structure at the active site is not a guarantee of structural conservation at other levels. Indeed, far-UV CD spectra of Mj-MAT revealed differences in secondary structure composition as compared with the E. coli and rat MAT I/III proteins. These changes correspond mainly to a large increase in helicity (53 vs. 19%) as determined by CD spectroscopy (Lopez-Vara et al. 2000; Lu and Markham 2002). Differences in secondary structure composition derived from far-UV CD data have also been described for other MATs with higher sequence conservation, and the variations may be ascribed to the presence of large insertions in loops (Gasset et al. 2002; Kamarthapu et al. 2008). Indeed, the number of residues in certain loops, such as that connecting β-strands A2 and A3, served to distinguish among eukaryotic and eubacterial sequences (Sanchez-Perez et al. 2004), whereas the core crystal structures remain alike (Takusagawa et al. 1996; Gonzalez et al. 2000; Markham and Pajares 2009).

Sequence and structural changes are expected to occur between mesophilic and thermophilic proteins in order for the latter to acquire their higher thermostability, with a combination of factors typically seeming to be responsible for this global effect. Several authors have suggested among the stabilizing determinants particularly, increases in the amount of hydrophobic and charged amino acids, changes in titratable groups (especially Glu and Lys) and shortening of the protein chain (Berezovsky et al. 2007; Glyakina et al. 2007; Greaves and Warwicker 2007). These proposals are only partially observed in the Mj-MAT sequence, which does show an increase in the percentage of charged residues (Glu and Lys especially), whereas a slight decrease in hydrophobic amino acid content is observed and the average length of the MAT chains is preserved (Sanchez-Perez et al. 2004; Garrido et al. 2009). Our ANS binding data indicate that the exposed apolar surface is very much reduced in native Mj-MAT as compared with the mammalian dimer (MAT III) or Bacillus subtilis MAT (BsMAT), which show high affinity for the dye (Gasset et al. 2002; Sanchez del Pino et al. 2002; Kamarthapu et al. 2008). In fact, native MAT III shows stronger binding of the dye than is exhibited by the monomeric equilibrium intermediate detected during its urea-unfolding (Gasset et al. 2002), and BsMAT moderately increases ANS

binding in early unfolding steps (Kamarthapu et al. 2008). Other means of acquiring higher stability may include: (a) covalent modifications, most of which are favored at elevated temperatures or extreme pHs; (b) increases in contact order or atom–atom contacts; and (c) increased packing and docking of domains. A detailed exploration of these possibilities is precluded due to the lack of a crystal structure for Mj-MAT, and the few analyses carried out to date have been based on sequence comparisons. To ameliorate this limitation, we developed a structural model using as template the coordinates for human MATα2 (pdb 2P02), which then allowed interpretation of urea-unfolding data (Garrido et al. 2009). For model construction, we selected the homologues with common fundamental characteristics such as using the same ligands or cofactors, preserving important residues (i.e. amino acids involved in catalysis), and sharing the predicted secondary structure. The main characteristics of the model structure are the conservation of the three-domain organization of MAT monomers, location of the residues involved in catalysis at the interface between monomers, and a change in the relative orientation between dimer subunits (Garrido et al. 2009). The single tryptophan (W387) of the wild type Mj-MAT appears to be located at the surface of the model; however, the lack of sequence homology at the C-terminus of the protein forced the Mj-MAT 3D-model to end at residue L388, thus diminishing confidence in the predicted environment of W387 since the final 18 residues are missing. Therefore, the difference between the experimental fluorescence λ_{max} (which is indicative of a buried residue) and the modeled location of W387 on the protein surface can be attributed to limitations of the model at the C-terminus. On the contrary, for the rest of the mutated residues their experimental λ_{max} values roughly coincide with the environments proposed in the model (Garrido et al. 2009). Thus, Y72, Y170 and Y344 appear at the monomer–monomer interface, whereas Y85, Y226, Y233, Y255, Y273 and Y371 are located at the protein surface, but close to the interface (Fig. 7). The aromatic rings of residues 120, 170, 226, 233, 255, 267, 323, 344 and 371 appear in apolar environments that correspond either to inside of the monomer or the intersubunit contact areas, whereas those of amino acids 49, 72, 85, 273 and 387 seem partially exposed to the solvent.

Mj-MAT was isolated from a methanogenic thermophilic archaeon, and hence was expected to show higher stability than mesophilic MATs. This expectation was confirmed by comparison of urea-denaturation data (Garrido et al. 2009) with those for mammalian MAT III (Gasset et al. 2002) and BsMAT (Kamarthapu et al. 2008). Mj-MAT retained an important percentage of secondary (40%) and tertiary structure even in the presence of 8 M urea and activity could still be measured at 6 M denaturant.

Fig. 7 Frontal and lateral views of the Mj-MAT dimer. The figure shows the location of the mutated residues in the structure of the Mj-MAT dimer using the coordinates of the model previously described (Garrido et al. 2009). Frontal (**a**) and lateral (**b**) views of the dimer are shown, where the molecular surface of subunit A (*dark grey*) is depicted together with the secondary structure elements of the monomer in subunit B (*light grey*), including the side chains of the aromatic residues (*black*)
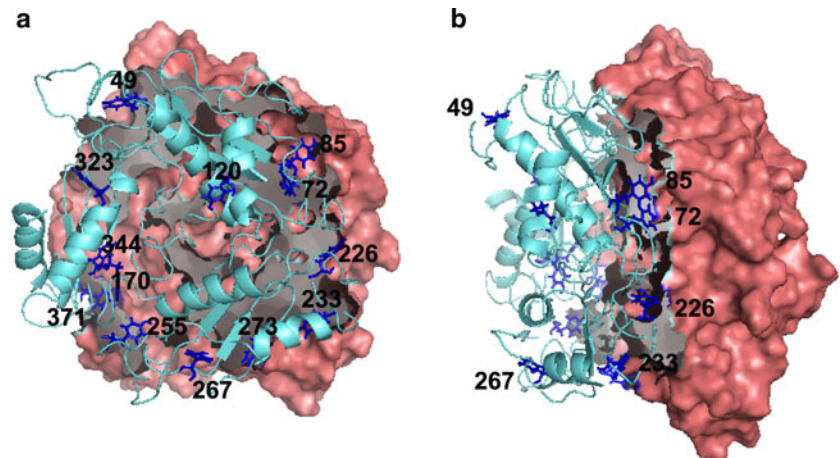
Total inactivation, the complete red shift displacement of the λ_{max} of W387, and the total loss of far-UV CD signature of Mj-MAT were only obtained using GCl as denaturant. The observation of two GCl unfolding transitions by far-UV CD and the tryptophan fluorescence suggests three-state behavior, as previously detected for urea denaturation of MAT III (Gasset et al. 2002). In contrast, previous Mj-MAT urea-unfolding results suggested a four-state process similar to that described for BsMAT (Kamarthapu et al. 2008; Garrido et al. 2009). Detection of 2- to 5-state processes during folding of oligomeric proteins seems common and involves intermediates with diverse association states (Neet and Timm 1994; Batey et al. 2006). The population of different kinds of intermediates, and hence their detection during unfolding, may depend on the denaturant used. Other characteristics that have been suggested to determine folding mechanisms are the protein size and composition. Indeed, Ma et al. indicate that proteins following three-state unfolding have on average 139 residues, and that multi-state folding occurs in proteins with composition-based folding type predictor (C_p) values larger than zero (Ma et al. 2007). Our results point out that Mj-MAT, as the rest of the MAT family of proteins, meets some of the premises mentioned above and shows the general behavior expected for multi-state folders.

Most of the activity loss induced by GCl occurs during the first transition, in coincidence with slight changes in the λ_{max} and early alterations in the hydrodynamic volume of the protein, which then elutes in a position that could be ascribed either to a compact dimer, a non-globular monomer or to an interconverting mixture of both species. Sedimentation velocity experiments identified two species with $s_{20,w}$ compatible with monomers ($\sim 30\%$) and compact dimers ($\sim 70\%$). The presence of residual activity while these changes are taking place confirms the dimeric structure of the intermediate J_2, since this oligomeric arrangement is needed for active site conservation (Markham and Pajares 2009). However, the percentage of activity

($\sim 15\%$) observed does not correspond to that of the dimeric species ($\sim 70\%$) detected, therefore suggesting subtle changes that affect the active site. These alterations may relate to a softening of the intersubunit interactions that would allow partial dissociation during centrifugation. Mesophilic MATs show similar changes at low urea concentrations (Gasset et al. 2002; Kamarthapu et al. 2008), and hence confirm the higher stability of the archaeal isoenzyme that follows a similar behavior only in the presence of a stronger denaturant.

Analysis of the activity results obtained from the mutants showed that the W387F–Y85W protein inactivates at lower GCl concentrations than the wild type enzyme. The possibility of salt effects was excluded since activity is preserved up to 4 M KCl. Such data suggest that this modification at the N-terminal of β-strand E3 makes the protein more susceptible to GCl inactivation. In contrast, urea exerts a wider effect and mutants at several loops (W387F–Y371W, W387F–Y267W), α-helices (W387F–Y233W) and β-strands (W387F–Y344W) loose activity at lower concentrations than the wild type (Garrido et al. 2009). This large activity reduction induced by low GCl concentrations does not correlate with structural changes of the wild type protein, a result that is in agreement with previous observations indicating that active sites tend to be located in regions that are more fragile toward denaturants than the whole protein (Tsou 1986). No secondary structure modifications are detected in this low denaturant range, whereas alterations in the tertiary structure around tryptophan residues 72 and 170 are observed. These are two of the mutants showing early changes during urea inactivation (W387F–Y72W, W387F–Y85W, W387F–Y170W, W387F–Y233W, W387F–Y273W, W387F–Y49W) (Garrido et al. 2009), and hence the data suggest their location in the most denaturant-susceptible structural elements.

Further increases in GCl concentration induce changes in hydrodynamic volume, sedimentation coefficient, ellipticity (53%) and the first transition in tryptophan

fluorescence. The significant loss of helicity may indicate a change of monomer shape, probably at the external surface where helical structures are located, while a small percentage of the initial activity is preserved. Loss of the remaining MAT activity in the presence of GCl occurs after initial modifications in tertiary structure around tryptophans 72, 170 and 255. Moreover, it takes place concomitantly with early changes around residues 233, 120, 226, 267, 273, 387, 323 and 371, and secondary alterations in the environment of amino acids 72 and 170. Thus, the changes produced in the GCl-induced J_2 intermediate that lead to high-Mr species (aggregation prone monomers) occur around basically the same microenvironments affected by urea-I_2 production (Garrido et al. 2009). The main difference arises from the higher degree of alteration around the C-terminal ends of E2 (W387F–Y72W) and E6 (W387F–Y170W) β-strands. These residues appear at the interface where the 3D-structural model predicts that monomers make contact (Fig. 7b), and hence the perturbation of their environments may reflect deep changes close to the active site.

A characteristic of oligomeric proteins is that they show protein concentration dependence when denaturation and dissociation reactions are coupled (Mallam and Jackson 2005). Therefore, the lack of protein concentration dependency of the fluorescence curves between 1.5–2 M GCl (first transition), together with increases in elution volumes and changes in $s_{20,w}$ values suggest that intermediate J_2 has a compact dimeric structure. Such an intermediate shows slight affinity for ANS in this denaturant range, where the plateau in activity is detected. This behavior suggests minimal exposure of hydrophobic patches as was previously described for the I_2 intermediate obtained with urea (Garrido et al. 2009), and which is in contrast to the apolar intermediate detected for mammalian MAT III (Gasset et al. 2002) and BsMAT (Kamarthapu et al. 2008). MAT III structure was shown to have an ANS binding motif at a hydrophobic cleft made by the sequences P358–G359 on one side and the hydrophobic side chains of V131–G132–A133 on the other (Sanchez del Pino et al. 2002). Such a motif is lacking in Mj-MAT, where secondary structure predictions only identified I139–G140–Q141 (Garrido et al. 2009).

The evolution of J_2 to high-Mr protein species takes place together with the last changes in the environments of residues 72, 120 and 273, as well as the initial modification around amino acid 49 according to fluorescence data. The extent of these alterations clearly differs from that observed at the same range of urea concentrations, where I_2 accumulates (Garrido et al. 2009). At that point urea only induces partial alterations in the environment around these residues, whereas GCl has completed its effects on the C-terminal end of E2 (W387F–Y72W) and the N-terminal

end of E9 (W387F–Y273W) β-strands, as well as on α-helix H2 (W387F–Y120W). In addition, three of the residues under study are transiently buried during disruption of the J_2 intermediate according to the fluorescence behavior observed with the mutants. These amino acids are located in β-strands of the central (E2, E3) and N-terminal domains (E9). Thus, GCl-J_2 arises from adjustments in areas related to buried residues, according to the 3D-model structure, and is disrupted when these same elements suffer additional alterations.

Dependence on protein concentration was observed during the second fluorescence transition (2.5–4 M), suggesting dimer dissociation at this step as described for other oligomeric systems (Gasset et al. 2002; Mallam and Jackson 2005). Previous results using urea showed that dissociation and final inactivation were obtained upon completion of the changes around α-helixes H1 (W387F–Y49W) and H6 (W387F–Y323W) and β-strands E9 and E12 (Garrido et al. 2009). In contrast, these residues suffer only partial alterations at the corresponding GCl step. GCl-induced dissociation renders monomers prone to aggregation, as deduced from the sedimentation velocity data and the chromatographic elution pattern. This process involves basically the same structural elements that are perturbed at high urea concentrations (>5.5 M) (Garrido et al. 2009), although the susceptibility to the denaturant shown by these secondary structure elements is not the same. Thus, α-helix H7 (W387F–Y371W) seems more susceptible to GCl than to urea, whereas loops connecting α-helix H5 with β-strands E8 (W387F–Y226W) and E9 (W387F–Y255W) seem more accessible to urea at this step. Differences in stability due to the chosen denaturant can be expected, as GCl adds salting effects to those induced by urea (Mayr and Schmid 1993; Akhtar et al. 2002). Direct interactions of guanidinium ions with charged species is also stronger than for urea, thus enhancing the protein denaturation efficiency of this agent as has been shown using small solutes in molecular dynamic simulations (O'Brien et al. 2007).

In summary, urea and GCl denaturation of Mj-MAT both allowed detection of dimeric intermediates, which showed perturbations in the environment of the same secondary structure elements. Independently of the denaturant chosen the less stable structures of the protein are β-strands E2 and E6. Neither the native nor the J_2-intermediate expose large portions of apolar surface to the solvent. Further denaturation of J_2 renders species prone to aggregation that, according to the available 3D-model of Mj-MAT and the behavior of the tryptophan mutants, arise from transient burial of some secondary structure elements. These are β-strands E2, E3 and E9, which are involved in the central and N-terminal domains of the monomer structure. Location of these strands at the dimer interface,

where the active sites are placed, suggests a severe modification of this area that may lead to softening of the monomer–monomer interactions, and hence activity loss and dissociation in a very narrow range of GCl concentration.

References

Akhtar MS, Ahmad A, Bhakuni V (2002) Guanidinium chloride- and urea-induced unfolding of the dimeric enzyme glucose oxidase. Biochemistry 41:3819–3827

Batey S, Scott KA, Clarke J (2006) Complex folding kinetics of a multidomain protein. Biophys J 90:2120–2130

Berezovsky IN, Zeldovich KB, Shakhnovich EI (2007) Positive and negative design in stability and thermal adaptation of natural proteins. PLoS Comput Biol 3:e52

Cantoni GL (1951) Activation of methionine for transmethylation. J Biol Chem 189:745–754

Cantoni GL (1975) Biological methylation: selected aspects. Annu Rev Biochem 44:435–451

Dolnick BJ, Angelino NJ, Dolnick R, Sufrin JR (2003) A novel function for the rTS gene. Cancer Biol Ther 2:364–369

Eisenberg MA, Stoner GL (1971) Biosynthesis of 7, 8-diaminopelargonic acid, a biotin intermediate, from 7-keto-8-aminopelargonic acid and S-adenosyl-L-methionine. J Bacteriol 108:1135–1140

Frey PA, Hegeman AD, Ruzicka FJ (2008) The Radical SAM Superfamily. Crit Rev Biochem Mol Biol 43:63–88

Fujiwara K, Ishihama Y, Nakahigashi K, Soga T, Taguchi H (2010) A systematic survey of in vivo obligate chaperonin-dependent substrates. EMBO J 59:1552–1511

Garrido F, Alfonso C, Taylor JC, Markham GD, Pajares MA (2009) Subunit association as the stabilizing determinant for archaeal methionine adenosyltransferases. Biochim Biophys Acta 1794:1082–1090

Gasset M, Alfonso C, Neira JL, Rivas G, Pajares MA (2002) Equilibrium unfolding studies of the rat liver methionine adenosyltransferase III, a dimeric enzyme with intersubunit active sites. Biochem J 361:307–315

Glyakina AV, Garbuzynskiy SO, Lobanov MY, Galzitskaya OV (2007) Different packing of external residues can explain differences in the thermostability of proteins from thermophilic and mesophilic organisms. Bioinformatics 23:2231–2238

Gonzalez B, Pajares MA, Hermoso JA, Alvarez L, Sufrin Garrido F, JR Sanz-Aparicio J (2000) The crystal structure of tetrameric methionine adenosyltransferase from rat liver reveals the methionine-binding site. J Mol Biol 300:363–375

Gonzalez B, Pajares MA, Hermoso JA, Guillerm D, Guillerm G, Sanz-Aparicio J (2003) Crystal structures of methionine adenosyltransferase complexed with substrates and products reveal the methionine-ATP recognition and give insights into the catalytic mechanism. J Mol Biol 331:407–416

Graham DE, Bock CL, Schalk-Hihi C, Lu ZJ, Markham GD (2000) Identification of a highly diverged class of S-adenosylmethionine synthetases in the archaea. J Biol Chem 275:4055–4059

Greaves RB, Warwicker J (2007) Mechanisms for stabilisation and the maintenance of solubility in proteins from thermophiles. BMC Struct Biol 7:18

Houry WA, Frishman D, Eckerskorn C, Lottspeich F, Hartl FU (1999) Identification of in vivo substrates of the chaperonin GroEL. Nature 402:147–154

Iloro I, Chehin R, Goni FM, Pajares MA, Arrondo JL (2004) Methionine adenosyltransferase alpha-helix structure unfolds at lower temperatures than beta-sheet: a 2D-IR study. Biophys J 86:3951–3958

Kamarthapu V, Rao KV, Srinivas PN, Reddy GB, Reddy VD (2008) Structural and kinetic properties of Bacillus subtilis S-adenosylmethionine synthetase expressed in Escherichia coli. Biochim Biophys Acta 1784:1949–1958

Laue TM, Shah BD, Ridgeway TM, Pelletier SL (1992) Computer-aided interpretation of analytical sedimentation data for proteins. In: Harding SE, Rowe AJ, Horton JC (eds) Analytical ultracentrifugation in biochemistry and polymer science. Royal Society of Chemistry, Cambridge, pp 90–125

Lopez-Vara MC, Gasset M, Pajares MA (2000) Refolding and characterization of rat liver methionine adenosyltransferase from Escherichia coli inclusion bodies. Protein Expr Purif 19:219–226

Lu ZJ, Markham GD (2002) Enzymatic properties of S-adenosylmethionine synthetase from the archaeon Methanococcus jannaschii. J Biol Chem 277:16624–16663

Ma BG, Chen LL, Zhang HY (2007) What determines protein folding type? An investigation of intrinsic structural properties and its implications for understanding folding mechanisms. J Mol Biol 370:439–448

Mallam AL, Jackson SE (2005) Folding studies on a knotted protein. J Mol Biol 346:1409–1421

Markham GD, Pajares MA (2009) Structure–function relationships in methionine adenosyltransferases. Cell Mol Life Sci 66:636–648

Mayr LM, Schmid FX (1993) Stabilization of a protein by guanidinium chloride. Biochemistry 32:7994–7998

Neet KE, Timm DE (1994) Conformational stability of dimeric proteins: quantitative studies by equilibrium denaturation. Protein Sci 3:2167–2174

Nishimura S, Taya Y, Kuchino Y, Oashi Z (1974) Enzymatic synthesis of 3-(3-amino-3-carboxypropyl)uridine in Escherichia coli phenylalanine transfer RNA: transfer of the 3-amino-acid-3-carboxypropyl group from S-adenosylmethionine. Biochem Biophys Res Commun 57:702–708

O'Brien EP, Dima RI, Brooks B, Thirumalai D (2007) Interactions between hydrophobic and ionic solutes in aqueous guanidinium chloride and urea solutions: lessons for protein denaturation mechanism. J Am Chem Soc 129:7346–7353

Sanchez del Pino MM, Perez-Mato I, Sanz JM, Mato JM, Corrales FJ (2002) Folding of dimeric methionine adenosyltransferase III: identification of two folding intermediates. J Biol Chem 277:12061–12066

Sanchez-Perez GF, Gasset M, Calvete JJ, Pajares MA (2003) Role of an intrasubunit disulfide in the association state of the cytosolic homo-oligomer methionine adenosyltransferase. J Biol Chem 278:7285–7293

Sanchez-Perez GF, Bautista JM, Pajares MA (2004) Methionine adenosyltransferase as a useful molecular systematics tool revealed by phylogenetic and structural analyses. J Mol Biol 335:693–706

Schuck P (2000) Size-distribution analysis of macromolecules by sedimentation velocity ultracentrifugation and Lamm equation modeling. Biophys J 78:1606–1619

Schuck P, Perugini MA, Gonzales NR, Howlett GJ, Schubert D (2002) Size-distribution analysis of proteins by analytical ultracentrifugation: strategies and application to model systems. Biophys J 82:1096–1111

Sufrin JR, Finckbeiner S, Oliver CM (2009) Marine-derived metabolites of S-adenosylmethionine as templates for new anti-infectives. Mar Drugs 7:401–434

Takusagawa F, Kamitori S, Misaki S, Markham GD (1996) Crystal structure of S-adenosylmethionine synthetase. J Biol Chem 271:136–147

Tsou CL (1986) Location of the active sites of some enzymes in limited and flexible molecular regions. Trends Biochem Sci 11:427–429

Van Lanen SG, Iwata-Reuyl D (2003) Kinetic mechanism of the tRNA-modifying enzyme S-adenosylmethionine:tRNA ribosyl-transferase-isomerase (QueA). Biochemistry 42:5312–5320